Chapter | six

Modeling Relative Motion Using Orbital Elements

I am a star fallen from the
Blue tent upon the green carpet.
I am the daughter of the elements
With whom Winter conceived.

Khalil Gibran (1883–1931)

In Chapter 4, we discussed the nonlinear, unperturbed, equations of relative motion in a rotating Cartesian coordinate system centered on the reference orbit. In Section 5.1 we developed the CW approximation, which utilized the same rotating coordinate system to derive expressions for the linear relative motion between satellites assuming that the reference orbit is circular. Recognizing some of the limitations of this approach, we presented generalizations of the CW equations for eccentric reference orbits (the TH equations) in Section 5.6.

An important modification of spacecraft relative motion modeling is the use of orbital elements as constants of unperturbed motion instead of the Cartesian initial conditions. This concept, originally suggested by Hill [118], has been widely used in the analysis of relative spacecraft motion [32,34,119]. One of the main advantages of the orbital-elements approach is the straightforward incorporation of orbital perturbations, yielding Lagrange's planetary equations (LPE) and the Gauss variational equations (GVE), introduced in Chapter 2. Moreover, utilizing orbital elements facilitates the derivation of high-order, nonlinear extensions to the CW solution in Cartesian coordinates.

There have been a few reported efforts to obtain high-order solutions to the relative motion problem. Karlgaard and Lutze proposed formulating the relative motion in spherical coordinates in order to derive second-order expressions [120]. The use of Delaunay elements (cf. Section 3.2) has also been proposed. For instance, Vaddi et al. derived differential equations in order to incorporate

Spacecraft Formation Flying; ISBN: 9780750685337

perturbations and high-order nonlinear effects into the modeling of relative dynamics [106].

In this chapter, we will establish a methodology for obtaining arbitrary high-order approximations to the relative motion between spacecraft by utilizing the Cartesian configuration space in conjunction with classical orbital elements [121,122]. In other words, we propose utilizing the known inertial expressions describing vehicles in elliptic orbits in order to obtain, using a Taylor series approximation, a time-series representation of the motion in a rotating frame, where the coefficients of the time series are functions of the orbital elements. We subsequently show that under certain conditions, this time-series becomes a Fourier series. More importantly, in the process of the derivation, there is no need to solve differential equations. This significant merit results directly from utilization of the known inertial configuration space. The high-order approximation we present also provides important insights into boundedness and commensurability of relative formation dynamics. A first-order approximation of the relative motion variables for circular orbits leads to Hill's solution. This solution is utilized to obtain a hybrid set of linear differential equations, explicit in the motion variables and also δa. The hybrid model has the advantage of modeling a significant portion of the nonlinear effects that constitute δa. The geometry of the Hill's solution also provides a means for establishing the initial conditions for PCOs.

6.1 GENERAL SOLUTION TO THE NONLINEAR RELATIVE MOTION EQUATIONS

The unperturbed nonlinear equations of relative motion, Eqs. (4.14)–(4.16), can be solved – in terms of true anomaly – due to the fact that the generating orbits are Keplerian. To see this, we will find an expression for $\boldsymbol{\rho}$ using consecutive Eulerian rotations and a translation.

Let $\mathscr{P}_1$ be a perifocal frame associated with the deputy's orbit (cf. Section 2.1). The initial step is to transform from $\mathscr{P}_1$ to $\mathscr{I}$ using three consecutive clockwise rotations conforming to the common $3-1-3$ sequence, as we have pointed out in Section 2.3. To that end, we define the line-of-nodes (LON) obtained from the intersection of the deputy's orbital plane and the inertial reference plane. The composite rotation, $T \in \mathrm{SO}(3)$, transforming any vector in $\mathscr{P}_1$ into the inertial frame $\mathscr{I}$, is given by [33,44]

$$T(\omega_1, i_1, \Omega_1) = \begin{bmatrix} \mathrm{c}_{\Omega_1}\mathrm{c}_{\omega_1} - \mathrm{s}_{\Omega_1}\mathrm{s}_{\omega_1}\mathrm{c}_{i_1} & -\mathrm{c}_{\Omega_1}\mathrm{s}_{\omega_1} - \mathrm{s}_{\Omega_1}\mathrm{c}_{\omega_1}\mathrm{c}_{i_1} & \mathrm{s}_{\Omega_1}\mathrm{s}_{i_1} \\ \mathrm{s}_{\Omega_1}\mathrm{c}_{\omega_1} + \mathrm{c}_{\Omega_1}\mathrm{s}_{\omega_1}\mathrm{c}_{i_1} & -\mathrm{s}_{\Omega_1}\mathrm{s}_{\omega_1} + \mathrm{c}_{\Omega_1}\mathrm{c}_{\omega_1}\mathrm{c}_{i_1} & -\mathrm{c}_{\Omega_1}\mathrm{s}_{i_1} \\ \mathrm{s}_{\omega_1}\mathrm{s}_{i_1} & \mathrm{c}_{\omega_1}\mathrm{s}_{i_1} & \mathrm{c}_{i_1} \end{bmatrix} \tag{6.1}$$

where i_1, Ω_1, ω_1 are the deputy's inclination, right ascension of the ascending node (RAAN) and argument of periapsis, respectively, and we have again used the compact notation $\mathrm{s}_x = \sin(x), \mathrm{c}_x = \cos(x)$. The next step is to transform from $\mathscr{I}$ to the chief's perifocal frame, $\mathscr{P}_0$, using the rotation matrix $T^T(\omega_0, i_0, \Omega_0)$, where i_0, Ω_0, ω_0 are the chief's inclination, RAAN and argument of periapsis, respectively. The transformation of the deputy's position

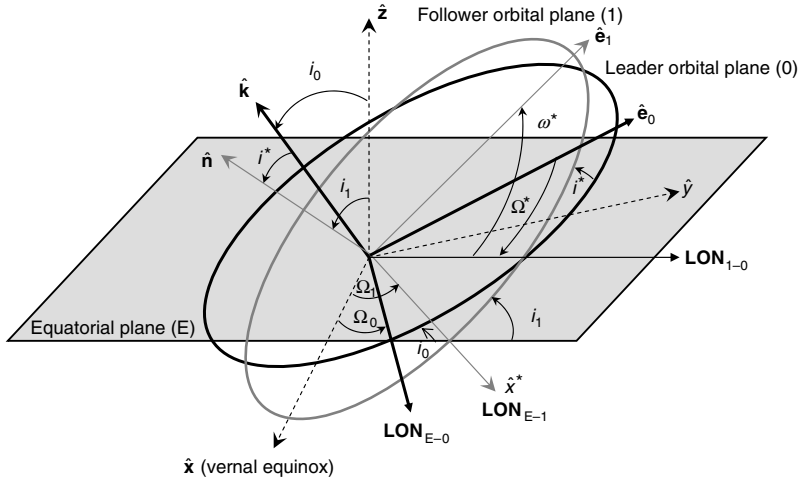

FIGURE 6.1 Relative orbital elements.

vector from $\mathscr{P}_0$ into $\mathscr{L}$, our standard rotating LVLH system centered at the chief, requires an additional rotation,

$$C(f_0) = \begin{bmatrix} c_{f_0} & s_{f_0} & 0 \\ -s_{f_0} & c_{f_0} & 0 \\ 0 & 0 & 1 \end{bmatrix}, \tag{6.2}$$

and a translation by $\mathbf{r}_0 = [r_0, 0, 0]^T$, resulting in

$$\boldsymbol{\rho} = C(f_0)T^T(\omega_0, i_0, \Omega_0)T(\omega_1, i_1, \Omega_1)[\mathbf{r}_1]_{\mathscr{P}_1} - \begin{bmatrix} r_0 \\ 0 \\ 0 \end{bmatrix} \tag{6.3}$$

where $[\mathbf{r}_1]_{\mathscr{P}_1}$ is the deputy's position vector in frame $\mathscr{P}_1$, expressed in terms of the deputy's eccentric anomaly, E_1, as (cf. Eq. (2.35))

$$[\mathbf{r}_1]_{\mathscr{P}_1} = \begin{bmatrix} a_1(\cos E_1 - e_1) \\ b_1 \sin E_1 \\ 0 \end{bmatrix} \tag{6.4}$$

and $b_1 = a_1\sqrt{1 - e_1^2}$.

Equation (6.3), written component-wise, is the most general solution (which still entails solution of Kepler's equation, as explained in the sequel) to the relative motion problem, modeled by the differential equations (4.14)–(4.16).

The obtained solution can be simplified if we utilize *relative orbital elements*. These orbital elements describe the orientation of the deputy's orbital plane relative to the chief's orbital plane, where the relative LON is defined by the intersection of these two planes, as shown in Fig. 6.1. Using this LON and

some fixed reference line – a good choice would be the eccentricity vector of the deputy's orbit, denoted by $\hat{\mathbf{e}}_1$ in Fig. 6.1 – we may define the relative RAAN, Ω^*, the relative argument of periapsis, ω^*, and the relative inclination, i^*. In terms of the relative elements, the expression for the relative position is simplified into

$$\boldsymbol{\rho} = C(f_0)T(\omega^*, i^*, \Omega^*) \begin{bmatrix} a_1(\cos E_1 - e_1) \\ b_1 \sin E_1 \\ 0 \end{bmatrix} - \begin{bmatrix} r_0 \\ 0 \\ 0 \end{bmatrix} \tag{6.5}$$

The matrix $T(\omega^*, i^*, \Omega^*)$ is calculated by substituting $(\omega_1, i_1, \Omega_1) \mapsto (\omega^*, i^*, \Omega^*)$ into Eq. (6.1), and $C(f_0)$ is given in (6.2). Some algebraic manipulations yield [122]

$$\begin{aligned} x = \frac{1}{2}\big[&(k_3 - k_2)\mathrm{s}_{f_0 - E_1} + (k_1 + k_4)\mathrm{c}_{f_0 - E_1} + (k_3 + k_2)\mathrm{s}_{f_0 + E_1} \\ &+ (k_1 - k_4)\mathrm{c}_{f_0 + E_1}\big] - e_1(k_3\mathrm{s}_{f_0} + k_1\mathrm{c}_{f_0}) - r_0 \end{aligned} \tag{6.6}$$

$$\begin{aligned} y = \frac{1}{2}\big[&-(k_1 + k_4)\mathrm{s}_{f_0 - E_1} + (k_3 - k_2)\mathrm{c}_{f_0 - E_1} + (k_4 - k_1)\mathrm{s}_{f_0 + E_1} \\ &+ (k_2 + k_3)\mathrm{c}_{f_0 + E_1}\big] + e_1(k_1\mathrm{s}_{f_0} - k_3\mathrm{c}_{f_0}) \end{aligned} \tag{6.7}$$

$$z = k_5(\mathrm{c}_{E_1} - e_1) + k_6\mathrm{s}_{E_1} \tag{6.8}$$

where

$$k_1 = (\mathrm{c}_{\Omega^*}\mathrm{c}_{\omega^*} - \mathrm{s}_{\Omega^*}\mathrm{s}_{\omega^*}\mathrm{c}_{i^*})a_1 \tag{6.9}$$

$$k_2 = (-\mathrm{c}_{\Omega^*}\mathrm{s}_{\omega^*} - \mathrm{s}_{\Omega^*}\mathrm{c}_{\omega^*}\mathrm{c}_{i^*})b_1 \tag{6.10}$$

$$k_3 = (\mathrm{s}_{\Omega^*}\mathrm{c}_{\omega^*} + \mathrm{c}_{\Omega^*}\mathrm{s}_{\omega^*}\mathrm{c}_{i^*})a_1 \tag{6.11}$$

$$k_4 = (-\mathrm{s}_{\Omega^*}\mathrm{s}_{\omega^*} + \mathrm{c}_{\Omega^*}\mathrm{c}_{\omega^*}\mathrm{c}_{i^*})b_1 \tag{6.12}$$

$$k_5 = \mathrm{s}_{\omega^*}\mathrm{s}_{i^*}a_1 \tag{6.13}$$

$$k_6 = \mathrm{c}_{\omega^*}\mathrm{s}_{i^*}b_1 \tag{6.14}$$

We can simplify Eqs. (6.6)–(6.8) by adopting the magnitude-phase representation

$$\begin{aligned} x = {} & K_1 \sin(f_0 - E_1 + \Phi_1) + K_2 \sin(f_0 + E_1 + \Phi_2) \\ & - K_3 \sin(f_0 + \Phi_3) - r_0 \end{aligned} \tag{6.15}$$

$$\begin{aligned} y = {} & K_1 \sin(f_0 - E_1 - \Phi_1) + K_2 \sin(f_0 + E_1 - \Phi_2) \\ & + K_3 \sin(f_0 - \Phi_3) \end{aligned} \tag{6.16}$$

$$z = K_4 \sin(E_1 + \Phi_4) - k_5 e_1 \tag{6.17}$$

where

$$K_1 = \frac{1}{2}\sqrt{(k_3 - k_2)^2 + (k_1 + k_4)^2} \tag{6.18}$$

$$K_2 = \frac{1}{2}\sqrt{(k_3 + k_2)^2 + (k_1 - k_4)^2} \tag{6.19}$$

$$K_3 = e_1\sqrt{k_1^2 + k_3^2} \tag{6.20}$$

$$K_4 = \sqrt{k_5^2 + k_6^2} \tag{6.21}$$

$$\Phi_1 = \tan^{-1}\frac{k_1 + k_4}{k_3 - k_2} \tag{6.22}$$

$$\Phi_2 = \tan^{-1}\frac{k_1 - k_4}{k_3 + k_2} \tag{6.23}$$

$$\Phi_3 = \tan^{-1}\frac{k_3}{k_1} \tag{6.24}$$

$$\Phi_4 = \tan^{-1}\frac{k_5}{k_6} \tag{6.25}$$

Thus, we have obtained the *general solution* for the nonlinear differential equations (4.14)–(4.16) modeling the relative motion problem. This general solution lies in the three-dimensional configuration space, comprising the *relative motion invariant manifold*, $\mathfrak{R}$. This manifold is invariant because any solution of the relative motion problem starting on $\mathfrak{R}$ will remain on $\mathfrak{R}$ for all times.

The dynamics on $\mathfrak{R}$ evolves according to Eq. (2.29) and a similar relationship that holds for the deputy's eccentric anomaly, emanating from Kepler's equation,

$$\dot{E}_1 = \frac{n_1}{1 - e_1\cos E_1} \tag{6.26}$$

where n_1 is the mean motion of the deputy. Thus, the general solution is a function of the chief's orbital elements, $\mathbf{oe}_0$, and the deputy orbital elements, $\mathbf{oe}_1$.

If the mean motions of the chief and deputy are commensurate (e.g. in a 1:1 resonance, i.e. $n_1 = n_0$, as discussed in Section 4.2), then the relative orbit will be a closed smooth curve $\gamma_c(t) \in \mathfrak{R}$ satisfying the periodicity condition with some period T, $\gamma_c(t) = \gamma_c(t + T)$. Otherwise, an open curve $\gamma_o(t) \in \mathfrak{R}$ will be obtained, and the motion will be quasi-periodic. Since the dynamics are always confined to evolve on $\mathfrak{R}$, the relative motion will be always bounded.[1]

Interestingly, in some cases, the manifold $\mathfrak{R}$ can be approximated by parametric representations of familiar geometric shapes. For example, when Ω^* and

[1] This observation is trivial, because the relative motion analyzed here is Keplerian. Nevertheless, many of the current works dealing with relative motion tend to distinguish between "bounded" and "unbounded" relative motion, while implicitly referring to 1:1 commensurable and non-commensurable motions, respectively.

ω^* are first-order small, the relative position components x, y, z constitute the parametric equations of an *elliptic torus*.[2] This issue is discussed in Section 6.3.

6.2 BOUNDS ON MAXIMAL AND MINIMAL DISTANCES

Gurfil and Kholshevnikov [122] developed a number of bounds on the distances between satellites flying on elliptic orbits, using the general solution of the relative motion problem discussed in the previous section. The methodology used in Ref. [122] distinguishes between the commensurable and non-commensurable cases. Some useful results are elaborated in this section.

6.2.1 The non-commensurable case

In the non-commensurable case, assuming circular chief and deputy orbits, the maximal and minimal distances correspond to extremal distances on the mutual LON, so that

$$\max \rho = a_0 + a_1, \qquad \min \rho = |a_0 - a_1|. \tag{6.27}$$

Given that the orbits of the chief and the deputy are coplanar and that the chief's orbit is circular, we distinguish between two cases. If

$$a_1(1 - e_1) \leq a_0 \leq a_1(1 + e_1). \tag{6.28}$$

then

$$\max \rho = a_0 + a_1(1 + e_1), \qquad \min \rho = 0 \tag{6.29}$$

Otherwise,

$$\max \rho = a_0 + a_1(1 + e_1) \tag{6.30}$$

$$\min \rho = \min\{|a_0 - a_1(1 - e_1)|, |a_0 - a_1(1 + e_1)|\} \tag{6.31}$$

6.2.2 The commensurable case

If the orbits of the chief and deputy satellites are circular and the motion is 1:1 commensurable, then for $i^* = 0$

$$\rho = 2a_1 \left| \sin \frac{(M_0)_0 - (M_0)_1}{2} \right| \tag{6.32}$$

where $(M_0)_0$ and $(M_0)_1$ are the respective mean anomalies at epoch of the chief and the deputy. For $i^* > 0$

$$\min \rho^2 = a_1^2(1 + \cos i^*)\{1 - \cos[(M_0)_0 - (M_0)_1]\} \tag{6.33}$$

$$\max \rho^2 = a_1^2\{3 - \cos i^* - (1 + \cos i^*) \cos[(M_0)_0 - (M_0)_1]\} \tag{6.34}$$

[2] A surface of revolution which is a generalization of the ring torus. It is produced by rotating an ellipse in the xz-plane about the z-axis.

which constitute particularly simple expressions for evaluating the extremal inter-vehicle distances.

6.3 RELATIVE MOTION APPROXIMATIONS WITH A CIRCULAR-EQUATORIAL REFERENCE ORBIT

In this section, we will use Eq. (6.5) to obtain time-series approximations of the relative motion in terms of classical orbital elements. To avoid unnecessary complications, we will assume that the reference orbit is circular and equatorial. To that end, we re-write Eqs. (4.74)–(4.76) (the differential equations modeling the deputy spacecraft dynamics relative to a circular reference orbit in the chief-fixed rotating LVLH frame $\mathscr{L}$) in vector form:

$$\frac{\mathrm{d}}{\mathrm{d}t}\begin{bmatrix}\boldsymbol{\rho}\\ \dot{\boldsymbol{\rho}}\end{bmatrix} = \begin{bmatrix}0_{3\times 3} & I_3\\ A_\rho & A_{\dot\rho}\end{bmatrix}\begin{bmatrix}\boldsymbol{\rho}\\ \dot{\boldsymbol{\rho}}\end{bmatrix} + \begin{bmatrix}0_{3\times 3}\\ I_3\end{bmatrix}\left[\frac{\mu \mathbf{r}_0}{a_0^3} - \frac{\mu(\boldsymbol{\rho}+\mathbf{r}_0)}{\|\boldsymbol{\rho}+\mathbf{r}_0\|^3}\right] \tag{6.35}$$

where

$$A_\rho = \begin{bmatrix}n_0^2 & 0 & 0\\ 0 & n_0^2 & 0\\ 0 & 0 & 0\end{bmatrix}, \qquad A_{\dot\rho} = \begin{bmatrix}0 & 2n_0 & 0\\ -2n_0 & 0 & 0\\ 0 & 0 & 0\end{bmatrix} \tag{6.36}$$

and $\mathbf{r}_0 = [a_0, 0, 0]^T$, a_0 is the radius of the chief's orbit, μ is the gravitational constant and $n_0 = \sqrt{\mu/a_0^3}$.

Recall that the CW approximate solutions for the configuration space over $\mathscr{L}$ were obtained in Section 5.1 by linearization of Eq. (6.35) about the origin, assuming that ρ/a_0 is first-order small. The resulting linear CW solution for the relative motion, given in Eqs. (5.17)–(5.19), can be equivalently written as

$$\begin{aligned}\boldsymbol{\rho}[t, \boldsymbol{\rho}(0), \dot{\boldsymbol{\rho}}(0)] = \tilde{\mathbf{C}}(0)[\boldsymbol{\rho}(0), \dot{\boldsymbol{\rho}}(0)] + \tilde{\mathbf{C}}_1[\boldsymbol{\rho}(0), \dot{\boldsymbol{\rho}}(0)]\cos(n_0 t)\\ + \tilde{\mathbf{S}}_1[\boldsymbol{\rho}(0), \dot{\boldsymbol{\rho}}(0)]\sin(n_0 t) + \tilde{\boldsymbol{\rho}}_d[t, \boldsymbol{\rho}(0), \dot{\boldsymbol{\rho}}(0)]\end{aligned} \tag{6.37}$$

where the constant vectors $\tilde{\mathbf{C}}_k$ and $\tilde{\mathbf{S}}_k$ are functions of the initial position and velocity in $\mathscr{L}$, and $\tilde{\boldsymbol{\rho}}_d \in \mathbb{R}^3$ is a non-periodic vector-valued function.

A selection of initial conditions that yield $\tilde{\boldsymbol{\rho}}_d \equiv 0$ renders the periodic terms in Eq. (6.37) a first-order *Fourier series*. Our objective is to generalize the topology of the linearized solution, in order to derive higher-order approximations via higher-order time-series expansions. To this end, we utilize classical orbital elements. This idea also permits a straightforward and natural incorporation of orbital perturbations and control forces via LPE or GVE, as will be discussed in Chapter 7.

To begin, let $\mathfrak{oe}_1 = [a_1, e_1, i_1, \Omega_1, \omega_1, (M_0)_1]^T$ be the classical orbital elements (cf. Eq. (2.42)) of a deputy spacecraft. Assuming that the reference orbit is circular and equatorial, i.e., coincides with the fundamental plane of the

inertial reference system, we use Eq. (6.5) to get

$$\boldsymbol{\rho} = \begin{bmatrix} x \\ y \\ z \end{bmatrix} = \frac{a_1(1-e_1^2)}{1+e_1\cos f_1} \begin{bmatrix} \mathrm{c}_{f_1+\omega_1}\mathrm{c}_{n_0t-\Omega_1} + \mathrm{c}_{i_1}\mathrm{s}_{f_1+\omega_1}\mathrm{s}_{n_0t-\Omega_1} \\ \mathrm{c}_{i_1}\mathrm{c}_{n_0t-\Omega_1}\mathrm{s}_{f_1+\omega_1} - \mathrm{c}_{f_1+\omega_1}\mathrm{s}_{n_0t-\Omega_1} \\ \mathrm{s}_{i_1}\mathrm{s}_{f_1+\omega_1} \end{bmatrix} - \begin{bmatrix} a_0 \\ 0 \\ 0 \end{bmatrix} \quad (6.38)$$

Equation (6.38) provides the general, nonlinear, expression for the relative position vector as a function of orbital elements and time in a rotating frame of reference centered on a circular, equatorial orbit. For $\Omega_1, \omega_1 \ll 1$, x, y, z are the parametric equations of an elliptic torus, meaning that Eq. (6.38) can be also written in the form

$$x = (\kappa_1 + \kappa_2 \cos v)\cos u \quad (6.39)$$

$$y = (\kappa_1 + \kappa_2 \cos v)\sin u \quad (6.40)$$

$$z = \kappa_3 \sin v \quad (6.41)$$

where $u, v \in [0, 2\pi]$ are functions of the eccentric anomaly.

Example 6.1. *Assume that the normalized semimajor axes* $a_0 = 1, a_1 = 1.02,$ *and* $e_1 = 0.1, i_1 = 15°, \Omega_1 = 5°, \omega_1 = (M_0)_1 = 0°$. *Simulate the deputy's orbit according to Eq.* (6.38).

In order to perform the simulation, we need to integrate a single differential equation (cf. Eq. (2.29)):

$$\dot{f}_1 = \sqrt{\frac{\mu}{a_1^3(1-e_1^2)^3}}(1+e_1\cos f_1)^2, \quad f_1(0) = 0$$

We then plug the time history of f_1 into Eq. (6.38) and plot the results. Figure 6.2 shows the xy-projection of the relative motion using the normalization $a_0 = n_0 = \mu = 1$. As a_0 and a_1 do not commensurate, the energy/period matching condition is violated, so we do not expect a periodic motion. Instead, we see that the motion is quasi-periodic. This is an additional form in which epicyclic motion manifests itself. The deputy spacecraft performs an epicyclic motion along the unit circle in the chief-fixed rotating frame. Thus, although the relative motion is not 1:1 commensurable, it is certainly bounded, as relative motion between elliptic Keplerian orbits will always remain bounded regardless of any particular selection of coordinates or resonance conditions. Figure 6.3 shows the three-dimensional motion and the torus which it lies upon. The motion clearly evolves along the torus. If we change the semimajor axis of the deputy spacecraft to match that of the chief, the drift will stop, and a closed relative orbit will result. The closed orbit lies, again, on the three-dimensional elliptic torus.

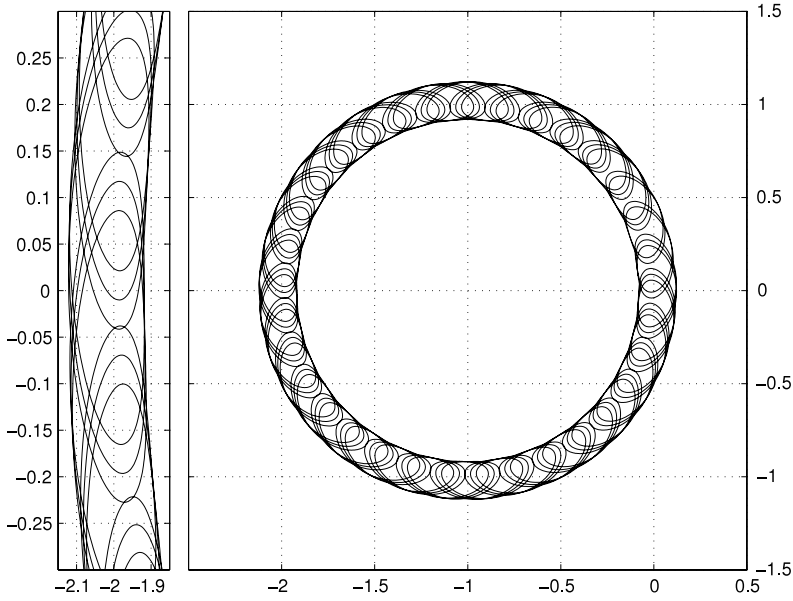

FIGURE 6.2 The xy-projection of an epicyclic motion of a deputy spacecraft in a chief-fixed rotating reference frame. The right pane shows the unit epicycle. The left pane presents a magnified view of an epicycle segment.

Although Eq. (6.38) may be used to investigate the relative dynamics of a spacecraft formation: It provides little insight into the relative dynamics since time dependence is implicit (due to the true anomaly-dependent terms). It is preferable to expand Eq. (6.38) into a time series of the form

$$\boldsymbol{\rho}(t, \mathbf{oe}_1, a_0) \approx \mathbf{C}_0(\mathbf{oe}_1, a_0) + \sum_{k=1}^{k_{\max}} [\mathbf{C}_k(\mathbf{oe}_1, a_0)\cos(kn_0 t) + \mathbf{S}_k(\mathbf{oe}_1, a_0)\sin(kn_0 t)] + \boldsymbol{\rho}_d(t, \mathbf{oe}_1, a_0) \tag{6.42}$$

where $\mathbf{C}_k$ and $\mathbf{S}_k$ are vector functions of the (possibly time-varying) orbital elements. Eq. (6.42) constitutes an orbital elements-based generalization of the first-order Cartesian parametrization (6.37). It will be shown shortly that Eq. (6.38) can indeed be represented in the form (6.42). We note that the drift term in Eq. (6.42), $\boldsymbol{\rho}_d$, stems from that fact that the Fourier series expansion of the relative motion is truncated at some $k_{\max} < \infty$. Due to the quasi-periodic nature of the relative orbit, $\boldsymbol{\rho}_d \equiv 0$ for $k_{\max} = \infty$.

6.3.1 High-order time-series approximations

For a circular and equatorial reference orbit, the orbital elements Ω_0 and ω_0 are undefined. We will therefore use instead the degenerate set of orbital elements $\mathbf{oe}_0 = [a_0, e_0, i_0, \varepsilon_0]^T$ where $\varepsilon_0 = \Omega_0 + \omega_0 - (M_0)_0$ is the mean

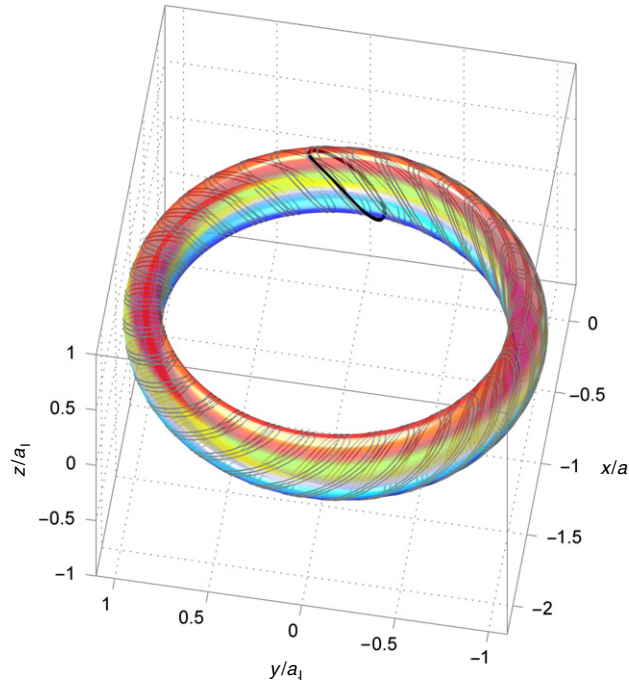

FIGURE 6.3 The relative motion orbits lie on an elliptic torus. Quasi-periodic motion is obtained without commensurability (dashed curve); a closed relative orbit is a result of orbital commensurability (solid curve).

longitude at epoch. In the derivation to follow, we utilize the normalization $a_0 = \mu = n_0 = 1$, resulting in the normalized reference orbital elements

$$\mathbf{oe}_0 = [1, 0, 0, 0]^T \tag{6.43}$$

The degenerate set of orbital elements for an arbitrary deputy spacecraft in the formation can be thus written as

$$\mathbf{oe}_1 = \mathbf{oe}_0 + \delta\mathbf{oe} \tag{6.44}$$

Therefore, the *orbital element differences* $\delta\mathbf{oe}$, also termed *differential orbital elements*, can be written in terms of the normalized deputy orbital elements as

$$\delta\mathbf{oe} = [\bar{a}_1 - 1, e_1, i_1, \varepsilon]^T = [\delta a, e, i, \varepsilon]^T \tag{6.45}$$

The analysis can be completed by expanding Eq. (6.38) into a Taylor series about $\mathbf{oe}_0$ in powers of $\delta\mathbf{oe}$. However, in order to obtain a time-series expansion of the form (6.42), we must first relate the deputy's true anomaly to time. This is performed by introducing the deputy's mean anomaly, M, and using the

following series expansion solution to Kepler's equation [33]:

$$f = M + 2\sum_{l=1}^{\infty}\frac{1}{l}\left[\sum_{s=-\infty}^{\infty} J_s(-le)\left(\frac{1-\sqrt{1-e^2}}{e}\right)^{|l+s|}\right]\sin(lM) \quad (6.46)$$

where $J_s(\cdot)$ is a Bessel function of the first kind[3] of order s. For illustration, for terms up to order e^2, Eq. (6.46) can be expanded as

$$f = M + 2e\sin M + \frac{5}{4}e^2\sin 2M + \mathcal{O}(e^3) \quad (6.47)$$

Based on Kepler's equation (2.26), let $\widetilde{M}_0 \triangleq n_0 t_0 - M_0$. Substituting

$$M = n_0 t - \widetilde{M}_0 = \sqrt{\frac{1}{(1+\delta a)^3}}\,t - \widetilde{M}_0 \quad (6.48)$$

into Eq. (6.47) yields the desired mapping $f \mapsto t$, which is then substituted into Eq. (6.38). The time-series expansion (6.42) is now available by writing a multi-variable Taylor series for the normalized relative position vector,

$$\begin{aligned}\boldsymbol{\rho}(t,\mathfrak{oe}_1) = \boldsymbol{\rho}(\mathfrak{oe}_0) + \sum_{l=1}^{\infty}\left[\frac{1}{l!}(\delta\mathfrak{oe}\cdot\nabla)^l\boldsymbol{\rho}(t,\mathfrak{oe})\right]_{\mathfrak{oe}=\mathfrak{oe}_0} &\approx \mathbf{C}_0(\mathfrak{oe}_1)\\ + \sum_{k=1}^{k_{\max}}[\mathbf{C}_k(\mathfrak{oe}_1)\cos(kt) + \mathbf{S}_k(\mathfrak{oe}_1)\sin(kt)] + \boldsymbol{\rho}_d(t,\mathfrak{oe}_1) &\quad (6.49)\end{aligned}$$

Note that the above expression is written assuming the normalization (6.43).

Based on Eq. (6.49), expressions for the relative motion between deputy spacecraft can be straightforwardly obtained [121].

6.3.2 Second-order approximation

Truncated to include the zero-, first- and second-order terms only, utilizing the identity

$$(\delta\mathfrak{oe}\cdot\nabla)(\delta\mathfrak{oe}\cdot\nabla)\boldsymbol{\rho}(t,\mathfrak{oe}) = \delta\mathfrak{oe}\cdot\nabla[\delta\mathfrak{oe}\cdot\nabla(\boldsymbol{\rho}(t,\mathfrak{oe}))] = \delta\mathfrak{oe}\cdot[\delta\mathfrak{oe}\cdot\nabla(\nabla\boldsymbol{\rho}(t,\mathfrak{oe}))]$$

Eq. (6.49) becomes

$$\begin{aligned}\boldsymbol{\rho}(t,\mathfrak{oe}_1) \approx\ & \boldsymbol{\rho}(\mathfrak{oe}_0) + (\delta\mathfrak{oe}\cdot\nabla_{\mathfrak{oe}})\boldsymbol{\rho}(t,\mathfrak{oe})|_{\mathfrak{oe}=\mathfrak{oe}_0}\\ &+\frac{1}{2}\delta\mathfrak{oe}\cdot[\delta\mathfrak{oe}\cdot\nabla_{\mathfrak{oe}}(\nabla_{\mathfrak{oe}}\boldsymbol{\rho}(t,\mathfrak{oe}))]|_{\mathfrak{oe}=\mathfrak{oe}_0} \quad (6.50)\end{aligned}$$

[3] Bessel functions of the first kind, denoted as $J_\alpha(x)$, are solutions of Bessel's differential equation. It is possible to define the function by its Taylor series expansion around $x = 0$: $J_\alpha(x) = \sum_{m=0}^{\infty}\frac{(-1)^m}{m!\Gamma(m+\alpha+1)}\left(\frac{x}{2}\right)^{2m+\alpha}$ where $\Gamma(z)$ is the gamma function.

Performing the symbolic calculation in Eq. (6.50), simplifying, and re-writing into the time-series (6.42) yields

$$\boldsymbol{\rho}(t, \boldsymbol{\alpha}_1) \approx \mathbf{C}_0(\boldsymbol{\alpha}_1) + \sum_{k=1}^{2} [\mathbf{C}_k(\boldsymbol{\alpha}_1)\cos(kt) + \mathbf{S}_k(\boldsymbol{\alpha}_1)\sin(kt)] + \boldsymbol{\rho}_d(t, \boldsymbol{\alpha}_1) \tag{6.51}$$

where, omitting the subscript 1 for brevity, we have

$$\mathbf{C}_0 = \begin{bmatrix} \delta a - \frac{1}{2}\varepsilon^2 - \frac{1}{4}i^2 - \frac{1}{2}e^2 \\ \varepsilon(1+\delta a) \\ -\frac{3}{2}ie\sin(\omega) \end{bmatrix} \tag{6.52}$$

$$\mathbf{C}_1 = \begin{bmatrix} 2\varepsilon e\sin(\widetilde{M}_0) - (1+\delta a)e\cos(\widetilde{M}_0) \\ -2(1+\delta a)e\sin(\widetilde{M}_0) - \varepsilon e\cos(\widetilde{M}_0) \\ i(1+\delta a)\sin(\omega - \widetilde{M}_0) \end{bmatrix} \tag{6.53}$$

$$\mathbf{S}_1 = \begin{bmatrix} -(1+\delta a)e\sin(\widetilde{M}_0) - 2\varepsilon e\cos(\widetilde{M}_0) \\ 2(1+\delta a)e\cos(\widetilde{M}_0) + \varepsilon e\sin(\widetilde{M}_0) \\ i(1+\delta a)\cos(\omega - \widetilde{M}_0) \end{bmatrix} \tag{6.54}$$

$$\mathbf{C}_2 = \begin{bmatrix} \frac{1}{4}i^2\cos\left[2(\omega - \widetilde{M}_0)\right] + \frac{1}{2}e^2\cos(2\widetilde{M}_0) \\ -\frac{1}{4}i^2\sin\left[2(\omega - \widetilde{M}_0)\right] - \frac{1}{4}e^2\sin(2\widetilde{M}_0) \\ \frac{1}{2}ie\sin(\omega - 2\widetilde{M}_0) \end{bmatrix} \tag{6.55}$$

$$\mathbf{S}_2 = \begin{bmatrix} -\frac{1}{4}i^2\sin\left[2(\omega - \widetilde{M}_0)\right] + \frac{1}{2}e^2\sin(2\widetilde{M}_0) \\ -\frac{1}{4}i^2\cos\left[2(\omega - \widetilde{M}_0)\right] + \frac{1}{4}e^2\cos(2\widetilde{M}_0) \\ \frac{1}{2}ie\cos(\omega - 2\widetilde{M}_0) \end{bmatrix} \tag{6.56}$$

The non-periodic terms are given by

$$\boldsymbol{\rho}_d = \begin{bmatrix} \frac{3}{2}\varepsilon\delta a t + \frac{3}{2}e\delta a\, t\sin(t - \widetilde{M}_0) - \frac{9}{8}\delta a^2 t^2 \\ -\frac{3}{2}\delta a t + \frac{3}{2}e\delta a\, t\cos(t - \widetilde{M}_0) + \frac{3}{8}\delta a^2 t \\ -\frac{3}{2}i\delta a\, t\cos(t + \omega - \widetilde{M}_0) \end{bmatrix} \tag{6.57}$$

Let us examine expressions (6.52)–(6.57). First, since $\mathbf{C}_0 \neq 0$, the center of motion of a deputy spacecraft in the rotating frame is offset relative to the reference orbit.

We can also make a few distinctions regarding the boundedness of the relative motion by examining the terms in $\boldsymbol{\rho}_d$. An interesting observation is that there exists a second-order secular drift in the out-of-plane direction for $\delta a \neq 0$. This phenomenon is not predicted by the CW approximation. It stems from the converging-diverging nature of the time series approximating the relative motion; if an infinite number of terms is taken in the approximation, we see convergence to the exact expression for the relative position vector (6.38), which is of course bounded if the spacecraft follows an elliptic Keplerian orbit (and periodic, if the orbital rates commensurate). We see here as well that if the energy matching condition is satisfied, i.e. $\delta a = 0$, then the relative motion is bounded.

6.3.3 First-order approximation: Hill's solutions

A first-order, CW-like solution written in terms of orbital elements, also known as *Hill's solution*, can be easily obtained by eliminating the second-order terms in Eqs. (6.52)–(6.57):

$$\mathbf{C}_0 = \begin{bmatrix} \delta a \\ \varepsilon \\ 0 \end{bmatrix} \tag{6.58}$$

$$\mathbf{C}_1 = \begin{bmatrix} -e\cos(\widetilde{M}_0) \\ -2e\sin(\widetilde{M}_0) \\ i\sin(\omega - \widetilde{M}_0) \end{bmatrix} \tag{6.59}$$

$$\mathbf{S}_1 = \begin{bmatrix} -e\sin(\widetilde{M}_0) \\ 2e\cos(\widetilde{M}_0) \\ i\cos(\omega - \widetilde{M}_0) \end{bmatrix} \tag{6.60}$$

$$\boldsymbol{\rho}_d = \begin{bmatrix} 0 \\ -\frac{3}{2}\delta a t \\ 0 \end{bmatrix} \tag{6.61}$$

Hill's solution may be compactly written using the magnitude-phase representation in dimensional form as

$$x(t) = \delta a - a_0 e\cos(n_0 t - \widetilde{M}_0) \tag{6.62}$$

$$y(t) = a_0\left[\varepsilon + 2e\sin(n_0 t - \widetilde{M}_0)\right] - \frac{3}{2}\delta a n_0 (t - t_0) \tag{6.63}$$

$$z(t) = a_0 i\sin(n_0 t + \omega - \widetilde{M}_0) \tag{6.64}$$

It is useful to compare the resulting relative motion components to the CW solution (5.17)–(5.19). Recall that the necessary and sufficient condition for stable linear motion using the CW equations was $\dot{y}(0) = -2nx(0)$ (cf. Eq. (5.23)), which is only a local condition for stability and is not generally related to the global condition for relative motion boundedness known as the

energy matching condition. However, in Hill's solution, the necessary and sufficient condition for stability is $\delta a = 0$, which is identical to the energy matching condition. Thus, interestingly, using orbital elements as constants of the motion have yielded a local stability condition which is identical to the global stability condition.

For $\delta a = 0$, Hill's solution becomes

$$x(t) = -a_0 e \cos(n_0 t - \widetilde{M}_0) \tag{6.65}$$

$$y(t) = a_0 \left[\varepsilon + 2e \sin(n_0 t - \widetilde{M}_0)\right] \tag{6.66}$$

$$z(t) = a_0 i \sin(n_0 t + \omega - \widetilde{M}_0) \tag{6.67}$$

Obviously, the xy-projection of the motion is a 2:1 ellipse centered at $(0, \varepsilon)$, having a semiminor axis e, a semimajor axis $2e$, and a constant eccentricity of $\sqrt{1 - e^2/4e^2} = \sqrt{3}/2$. This result should sound familiar; we made the exact same observation in Section 5.1 regarding the CW solution. The advantage of using orbital elements is that the geometric properties of the relative motion are well understood, constituting a much more natural and convenient approach for analyzing both unperturbed and perturbed relative dynamics.

It is also easy to see that if $\delta a = \omega = 0$ and $e = i$, Hill's solution yields a circular xz-projection having radius e. If $i = 2e$ and $\omega = \pi/2$, than the yz-projection is a circle with radius $2e$. Similar observations were made regarding the CW solution.

One should be careful, though, when relating the CW solution to Hill's solution, as the resulting relationships between the Cartesian initial conditions and orbital elements hold only locally. Different relationships will be obtained for higher-order solutions.

Example 6.2. *Simulate the motion of a deputy spacecraft with (the semimajor axis is written in normalized units)*

$$a_1 = 1, \delta a = 0, e = 0.02, i = 15^\circ, \Omega = 5^\circ, \omega = \widetilde{M}_0 = 0^\circ$$

relative to a circular equatorial orbit.

Figure 6.4 depicts a comparison of the exact, nonlinear solution (6.38), the second-order approximation (6.52)–(6.57) and Hill's solution (6.62)–(6.64). Notably, the second-order approximation is considerably closer to the exact solution, as Hill's approximation is limited to small relative inclinations and eccentricities.

6.4 ESTABLISHING THE PCO INITIAL CONDITIONS

Equations (6.62)–(6.64) can also be written in terms of the differential nonsingular elements [75] as

$$x = \delta a - a_0 \left[(\cos\theta)\delta q_1 + (\sin\theta)\delta q_2\right] \tag{6.68a}$$

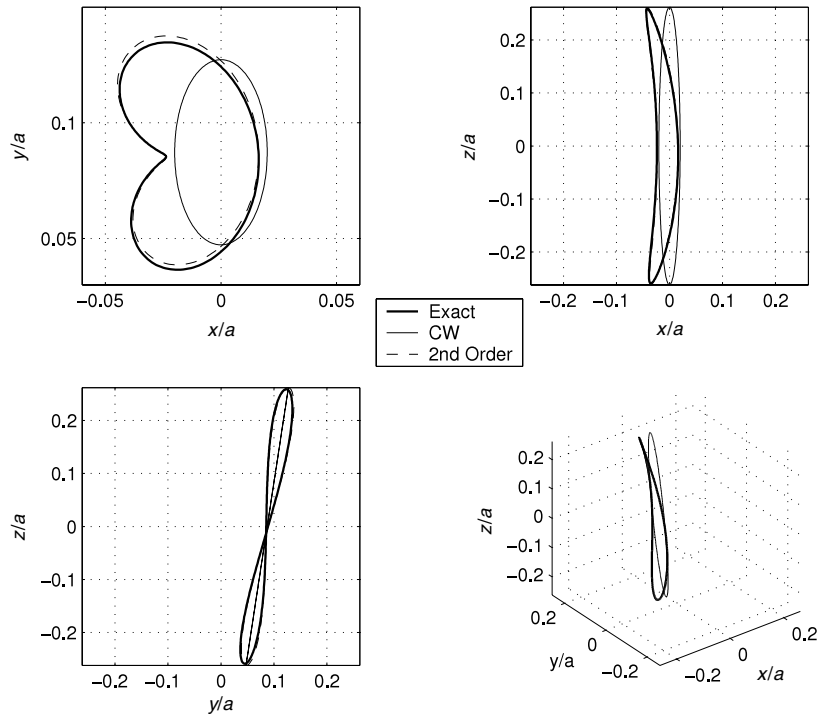

FIGURE 6.4 Motion of a deputy spacecraft in the reference-orbit centered rotating frame: Comparison of exact, first-, and second-order approximations.

$$y = -\frac{3}{2}n_0(t - t_0)\delta a + a_0\left[(\delta\lambda + \delta\Omega\cos i) + 2(\sin\theta)\delta q_1 - 2(\cos\theta)\delta q_2\right] \tag{6.68b}$$

$$z = a_0\left[(\sin\theta)\delta i - (\cos\theta\,\sin i)\delta\Omega\right] \tag{6.68c}$$

where δq_1, δq_2, $\delta\lambda$, $\delta\Omega$ and δi are the initial values of the respective differential orbital elements, and they remain constant for the two-body problem.

It can be shown that the differential nonsingular element initial conditions for obtaining a PCO of radius ρ and phase angle α, satisfying Eqs. (5.24)–(5.26) and Eq. (5.36), are [123]

$$\delta a = 0 \tag{6.69}$$

$$\delta q_1 = -\left(\frac{\rho}{2a_0}\right)\sin\alpha \tag{6.70}$$

$$\delta q_2 = -\left(\frac{\rho}{2a_0}\right)\cos\alpha \tag{6.71}$$

$$\delta i = \left(\frac{\rho}{a_0}\right)\cos\alpha \tag{6.72}$$

$$\delta\Omega = -\left(\frac{\rho}{a_0}\right)\left(\frac{\sin\alpha}{\sin i_0}\right) \tag{6.73}$$

$$\delta\lambda = \left(\frac{\rho}{a_0}\right)\cot i_0 \sin\alpha \tag{6.74}$$

Equations (6.69)–(6.74) constitute extremely useful relations for establishing PCOs and have been used in many of the example problems in this book, with a slight modification to the condition on δa, required to accommodate the effect of J_2. An alternative form of the set of PCO initial conditions, valid for near-circular orbits, is provided in Section 8.5. In the following section a set of approximate, linearized equations are developed for a direct simulation of relative motion in the $\mathscr{L}$ frame. These equations utilize both the orbital elements and the Cartesian relative motion states.

6.5 HYBRID DIFFERENTIAL EQUATIONS WITH NON-LINEARITY COMPENSATION FOR UNPERTURBED CIRCULAR ORBITS

A linear periodicity condition for relative motion with respect to an elliptic orbit was discussed in Chapter 5 in the context of the two-body STM. In this section, a set of *hybrid differential equations* of relative motion are derived for a two-body circular reference orbit. These equations are termed hybrid because they not only involve the LVLH states explicitly, but also δa, the differential semimajor axis as a parameter. Hence, they require a consistency between their initial conditions and δa of the deputy with respect to the chief. The variables x and z in Eqs. (6.68a)–(6.68c) contain periodic terms; they can be conveniently represented by second-order differential equations. The expression for y is handled in a different manner due to the presence of a secular term. Differentiation of Eq. (6.68b) with respect to time results in

$$\dot{y} = -\frac{3}{2}n_0\delta a + 2a_0 n_0\left[(\cos\theta)\delta q_1 + (\sin\theta)\delta q_2\right] \tag{6.75}$$

The above equation can be simplified by substituting Eq. (6.68a) to obtain

$$\dot{y} = \frac{1}{2}n_0\delta a - 2n_0 x \tag{6.76}$$

The equations for x and y can also be manipulated as shown below:

$$\ddot{x} = -{n_0}^2(x - \delta a) \tag{6.77}$$

$$\ddot{z} = -{n_0}^2 z \tag{6.78}$$

Equations (6.76)–(6.78) reproduce the results of Eqs. (6.68a)–(6.68c) for a consistent set of initial conditions. Even though only five differential equations are included in the derived model, information regarding the initial condition on $\dot{y}$ is required to compute δa. An exact analytical expression for δa in terms

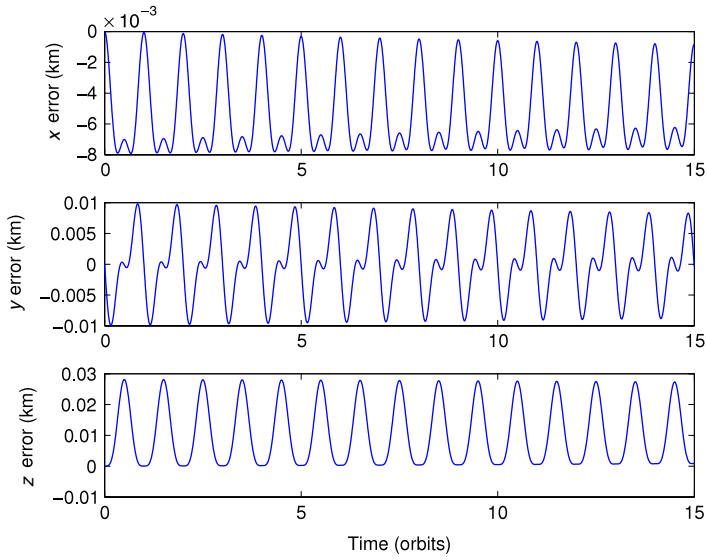

FIGURE 6.5 Errors between the linear and nonlinear propagations ($\rho = 10$ km, $\alpha = 0°$, $\delta a = 0$).

of the relative motion states can be obtained from the equations of two-body motion [90]. Substitution of Eq. (5.66) into Eq. (6.77) results in the radial component of the CW equations. However, the actual δa cannot always be represented accurately by a linear approximation, especially when a long-term propagation is required. The use of the exact or higher-order approximate values of δa incorporates some of the nonlinear effects not captured by the CW equations. Equations (6.76)–(6.78) do not include the effects of perturbations or control inputs, which may cause changes in δa.

Example 6.3. *Compare the results produced by Eqs. (6.76)–(6.78) and a nonlinear simulation, with consistent sets of initial conditions. The following initial orbital elements of the chief are selected:*

$$a_0 = 7100 \text{ km}, \quad \theta_0 = 0, \quad i_0 = 70°$$
$$q_{10} = 0, \quad q_{20} = 0, \quad \Omega_0 = 45°$$

The PCO initial conditions are selected for the deputy. The orbital elements of the chief and deputy are converted into their respective ECI position and velocity states for the nonlinear simulation. A transformation of the relative initial states from the ECI to LVLH frames is used to obtain the required initial conditions for Eqs. (6.76)– (6.78).

Figure 6.5 shows the errors between the results produced by the linear model and a nonlinear simulation, for a PCO with $\rho = 10$ km and $\alpha_x = \alpha_z \equiv \alpha = 0$. Figure 6.6 shows the same for $\rho = 10$ km and $\alpha = 90°$. For both of these examples, $\delta a = 0$. The next set of figures (Figs. 6.7 and 6.8) show the errors

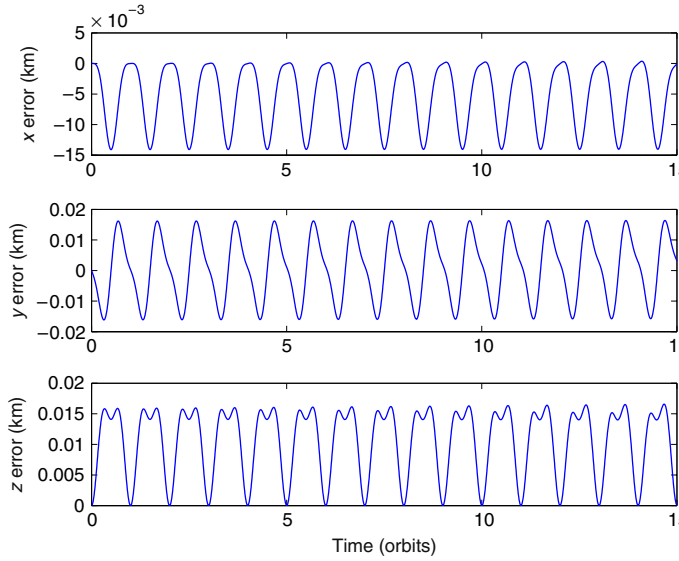

FIGURE 6.6 Errors between the linear and nonlinear propagations ($\rho = 10\,\text{km}$, $\alpha = 90°$, $\delta a = 0$).

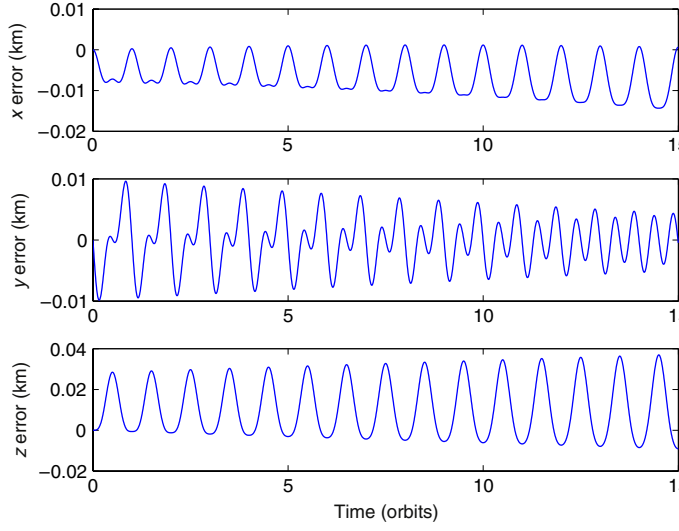

FIGURE 6.7 Errors between the linear and nonlinear propagations ($\rho = 10\,\text{km}, \alpha = 0°$, $\delta a = 50\,\text{m}$).

for $\delta a = 50$ m. As can be seen from these figures, the use of δa in the linear model compensates for a significant portion of the nonlinear effects, even for large relative displacements.

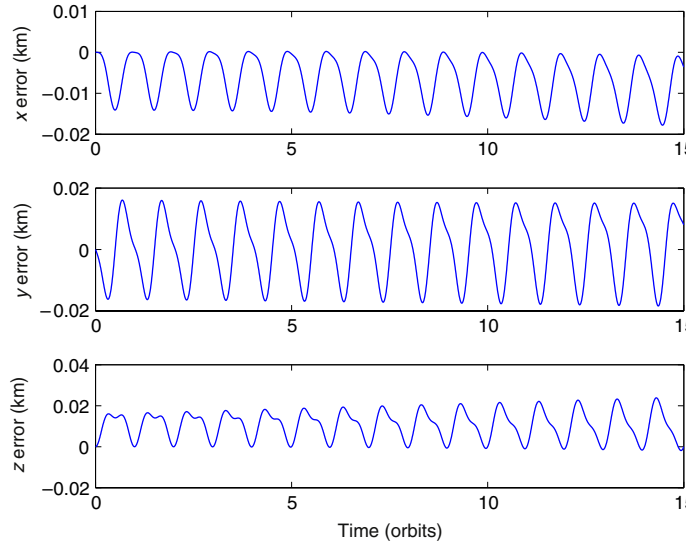

FIGURE 6.8 Errors between the linear and nonlinear propagations ($\rho = 10$ km, $\alpha = 90°, \delta a = 50$ m).

SUMMARY

We have written general expressions modeling the relative spacecraft geometry and have explicitly parameterized the relative motion configuration space using classical orbital elements as constants of the unperturbed Keplerian motion. Based on this geometric insight, we presented analytic expressions for a few bounds on the relative distances, which are important for generating safe and reliable spacecraft formations. These expressions are different for the commensurable and incommensurable cases.

The relative motion geometry evolves on an invariant manifold, which can be easily characterized using relative orbital elements. The motion along this manifold is quasi-periodic in the general case and periodic in the commensurable case. Both types of motion evolve on the relative motion manifold.

We also presented a framework for approximating the relative dynamics of spacecraft formations utilizing the known three-dimensional inertial solutions. The time-series parametrization of the relative position vector lends itself naturally to high orders and hence constitutes a useful analysis and modeling tool, providing much insight into the relative dynamics of spacecraft formations.

Finally, we discussed the process for setting up PCO initial conditions and derived a hybrid differential equation model for relative motion with a circular reference orbit. These equations involve the states in the $\mathscr{L}$ frame and the differential semimajor axis as a parameter.